CHAPTER 3

Al^{3+} ion capacitor with vanadium oxy-acetylacetonate and polyaniline

Al^{3+} ion capacitor with vanadium oxy-acetylacetonate and polyaniline

3.1 Introduction

In the previous chapter, the electrochemical investigation on Al^{3+} ion storage in to MoO_3 using aqueous and gel electrolytes was carried out. However, there are also some other promising electrode materials like organic and organic-inorganic hybrid materials which can store metal ions [1, 2]. For example, polyaniline (PANI) is an organic material which can electrochemically accommodate Al^{3+} ion [3]. Similarly, organic-inorganic hybrid materials such as vanadyl ethylene glycolate are investigated for Li^+ and Zn^{2+} ion storage [4, 5]. The Al^{3+} ion storage behavior of vanadyl ethylene glycolate is also illustrated recently [2]. Another interesting organic-inorganic hybrid material is vanadium oxy-acetylacetonate (abbreviated as VOA). It is a complex compound of vanadyl group (VO^{2+}) and two acetylacetonate anions. Wang et al. investigated it as an anode material for Li-ion battery [6]. But, to the best of our knowledge, there is no study which illustrates the Al^{3+} ion storage in VOA. Herein, we investigated the Al^{3+} ion electrochemistry of vanadium oxy-acetylacetonate in aqueous electrolyte and evaluated the electrochemical performance of an asymmetric supercapacitor with VOA and PANI as electrodes.

3.2 Experimental Section

3.2.1 Materials

Vanadium oxy-acetylacetonate ($VO(C_5H_7O_2)_2$) and Polyvinylidene fluoride (PVDF) were purchased from (Sigma Aldrich). Aniline, Ammonium peroxodisulfate, Hydrochloride acid (HCl), Aluminium chloride anhydrous powder, Aluminuim sulphate 16-hydrate and Aluminium nitrate monohydrate were obtained from (Merck). Carbon black and N-methyl-2-pyrrolidone were collected from (Alfa Aesar) and Distilled water.

3.2.2 Synthesis

3.2.2.1 *Synthesis of polyaniline*

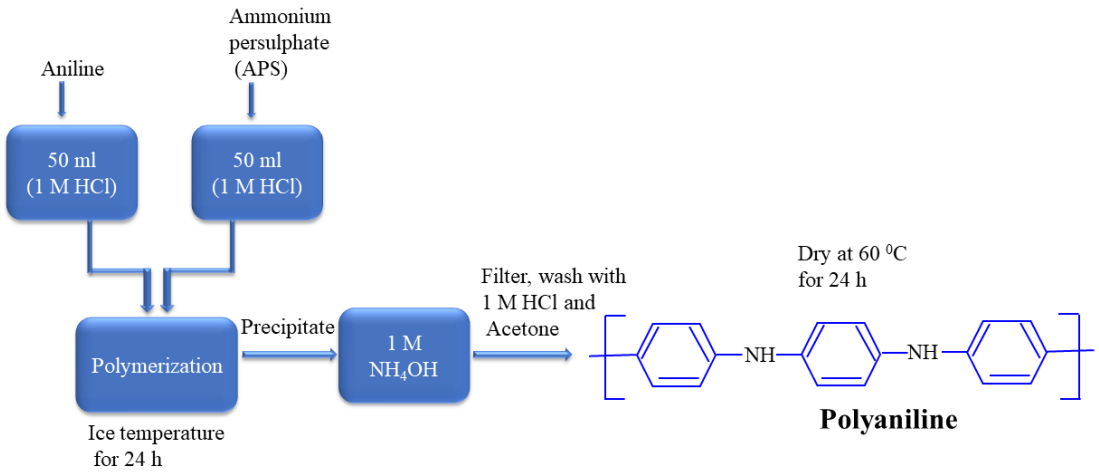

Figure 3.1: Schematic diagram of synthesis of polyaniline.

As shown in the above schematic diagram (Figure 3.1), polyaniline (abbreviated as PANI) was synthesized by a conventional polymerization method [7, 8]. In brief, 2 g of aniline was added to 50 ml of 1 M HCl under constant stirring for 30 min. Simultaneously, 4 g of ammonium peroxodisulfate was dissolved in 1 M HCl (50 ml) and this mixture was then added dropwise to the aniline/HCl mixture under constant stirring at ice bath temperature for 24 h. Thereafter, the precipitate was stirred with 1 M NH_4OH for 24 h. The resultant mixture was filtered and washed with 1 M HCl/acetone and dried at 60 ^oC for 24 h.

3.2.2.2 *Synthesis of vanadium oxy-acetylacetonate*

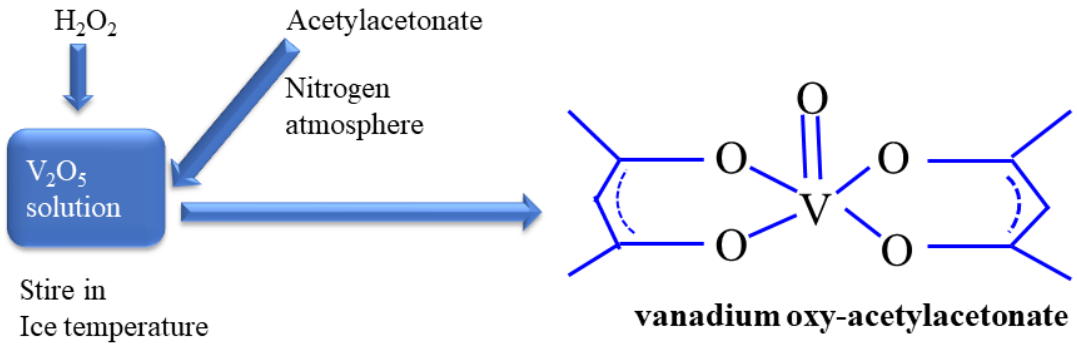

Figure 3.2: Schematic diagram of synthesis of vanadium oxy-acetylacetonate.

As displayed in the above schematic diagram (Figure 3.2), vanadium oxy-acetylacetonate (abbreviated as VOA) can be synthesized by standard solution based

method reported in the literature [6]. But due to lack of nitrogen atmosphere facility, vanadium oxy-acetylacetonate was procured from Sigma Aldrich (Product # 1003273459) and directly employed for the electrochemical analysis without any additional processing.

3.2.3 Characterizations

The crystallographic structures of the obtained materials were analyzed by powder X ray diffraction (BRUER AXS D8 FOCUS, Cu-$K_\alpha$radiation; $\lambda = 1.5406\dot{A}$) and Raman spectroscopy (RENISHAW BASIS SERIES WITH 515 LASER, RENISHAW, UK). The surface morphology was analyzed using scanning electron microscope (FESEM, JEOL, JSM7200F).

3.2.4 Electrochemical Analysis

Using N-methyl-2-pyrrolidone (NMP) as a drop coating medium, a homogenous slurry of VOA or PANI, carbon black and PVDF in a weight ratio of 8:1:1 was prepared and drop coated on a graphite paper and the electrodes were dried at 90 ^oC for 12 h. The utilized electrolytes were aqueous 1 M $AlCl_3$, 0.5 M $Al_2(SO_4)_3$, and 1 M $Al(NO_3)_3$. The preliminary electrochemical tests are conducted in a three-electrode system with Ag/AgCl, Pt, and VOA or PANI as reference, counter and working electrodes respectively. For asymmetric supercapacitor experiments, the two working electrodes are VOA and PANI. A mass balance of the two electrodes was maintained while evaluating the asymmetric supercapacitor.

3.3 Results and discussion

Figure 3.3a and 3.3c represents the XRD patterns of VOA and PANI respectively. All the diffraction peaks are similar to the previous report on VOA [$VO(C_5H_7O_2)_2$] [6]. There are few small intensity diffraction peaks from vanadium acetylacetonate also [$V(C_5H_7O_2)_3$]. The miller indices are obtained using VESTA software. The XRD pattern of PANI shows small intensity diffraction peaks identified as (011), (020) and (200). The FESEM image of VOA (Figure 3.3b) indicates random shaped agglomerates, whereas nanofibrous morphology could be seen for PANI (Figure 3.3d). Raman and FTIR spectra also confirm the formation of PANI (Figure 3.4 (a-b)).

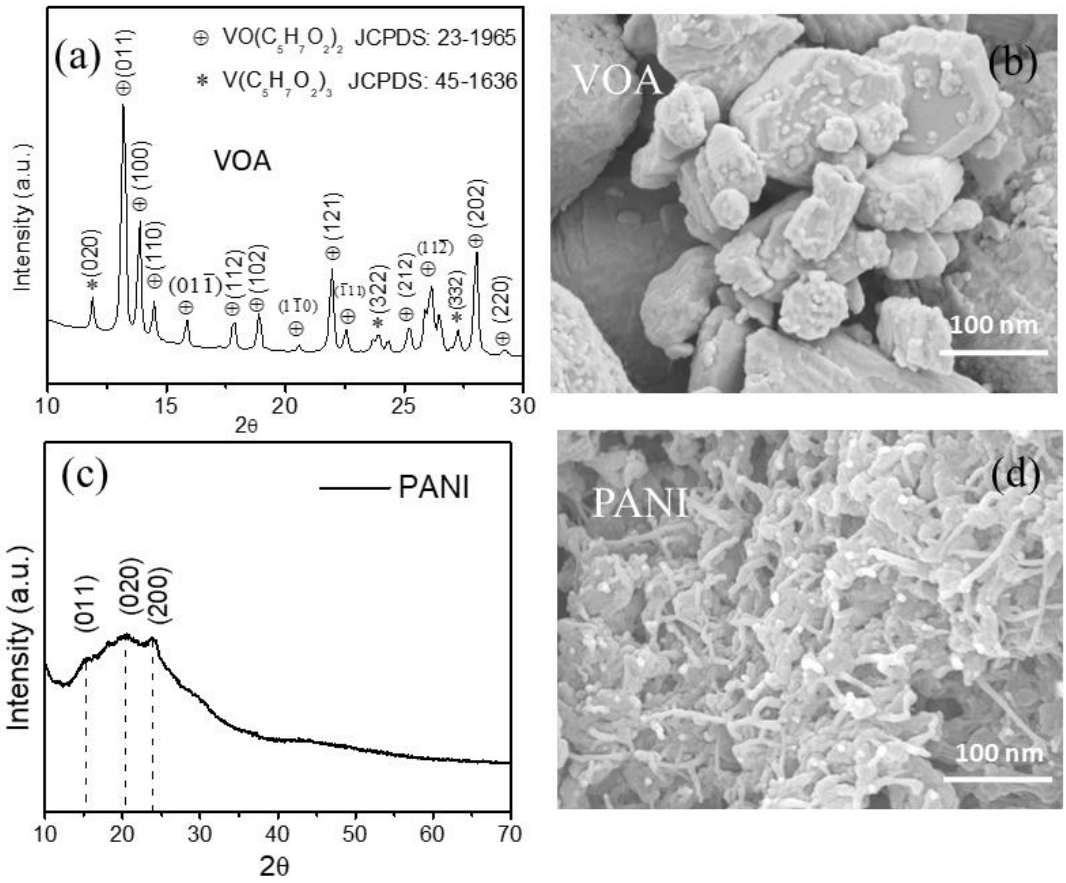

Figure 3.3: XRD pattern and FESEM image of (a, b) VOA and (c, d) PANI respectively.

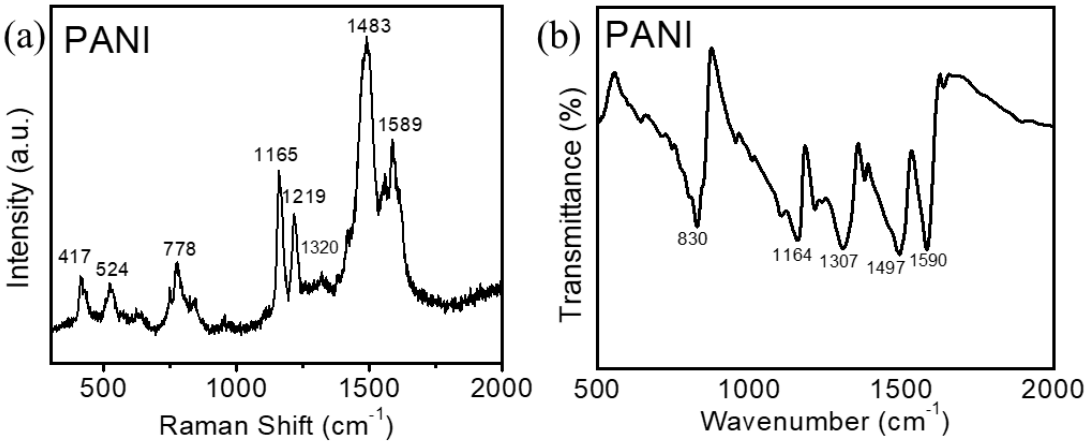

Figure 3.4: (a) Raman and (b) FTIR spectra of PANI.

Now, to study the electrochemical behavior, initially electrochemical experiments were performed in a three electrode set up. Figure 3.5a shows the cyclic voltammetry (CV) profiles of VOA in the potential window of -1 V to 0.3 V (vs Ag/AgCl) at a scan rate of 2 mVs^{-1} in 1 M $AlCl_3$ aqueous electrolyte. It could be observed that there are two pairs of very broad cathodic and anodic peaks. The

cathodic peaks are approximately located at -0.36 V (peak A) and -0.63 V (peak B), while the anodic peaks are noticed at -0.42 V (peak C) and 0.05 V (peak D). The CV profiles of VOA are almost similar even in the 0.5 M $Al_2(SO_4)_3$ aqueous electrolyte (Figure 3.5b). Contrarily, no noticeable electrochemical activity could be noticed in the 1 M $Al(NO_3)_3$ electrolyte (Figure 3.5c). Figure 3.6a shows the galvanostatic charge-discharge profiles of VOA at a current density of 1 Ag^{-1} in 1 M $AlCl_3$ aqueous electrolyte. Complementing the CV profiles, the charge-discharge profiles did not exhibit any prominent potential plateaus. However, considerable specific capacitance is obtained. The initial discharge specific capacitance is 392 Fg^{-1} and after initial decline in capacitance, it becomes stable in the subsequent cycles. The specific capacitance after 50 cycles is 182 Fg^{-1} (Figure 3.6b).

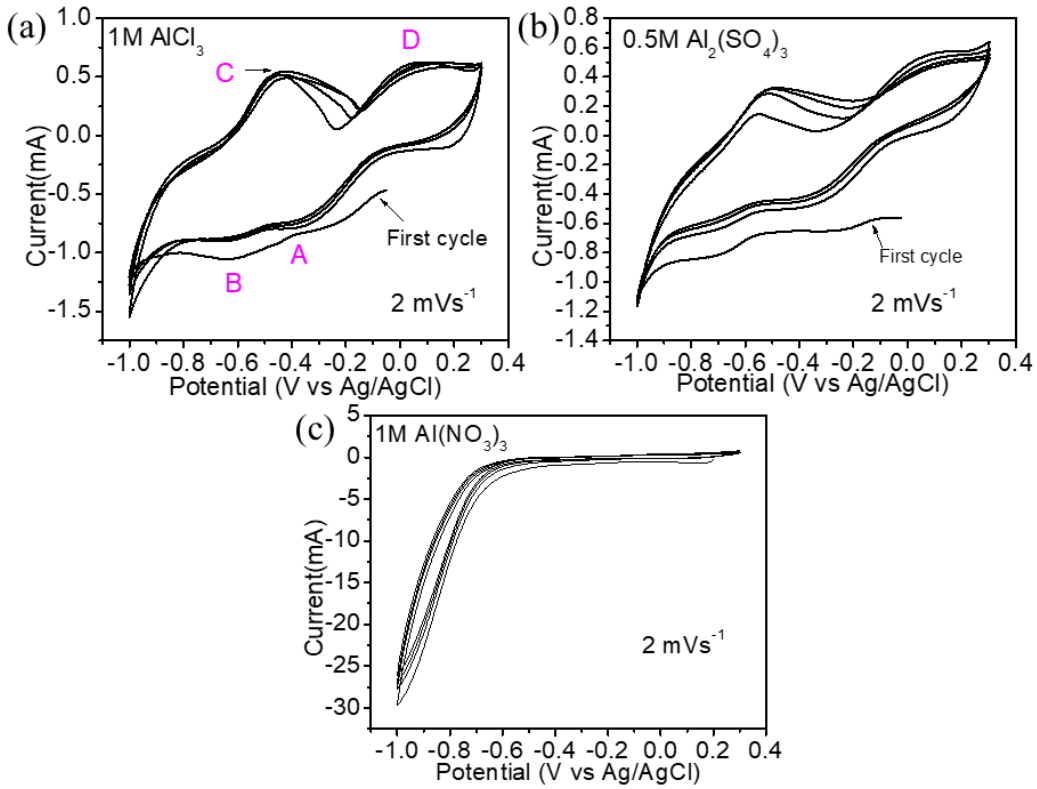

Figure 3.5: CV profiles of VOA in (a) 1 M $AlCl_3$, (b) 0.5 M $Al_2(SO_4)_3$ and (c) 1 M $Al(NO_3)_3$ aqueous electrolytes.

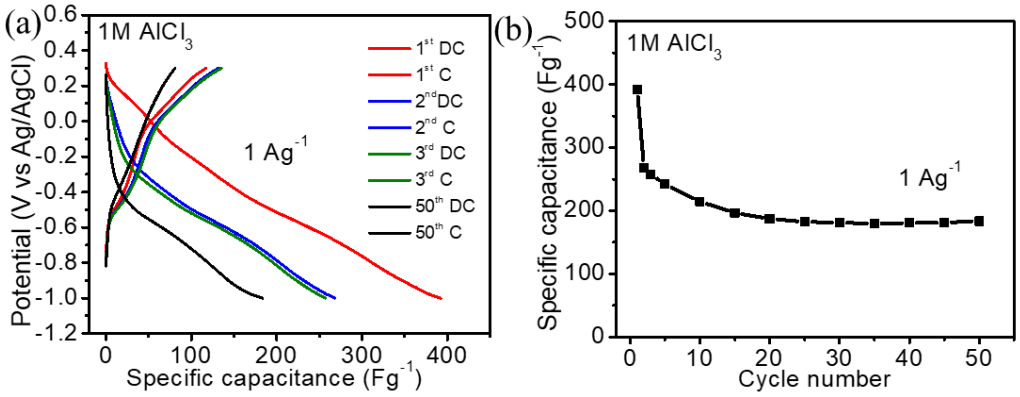

Figure 3.6: Charge-discharge profile of (a) VOA and (b) capacity versus cycle number of VOA in 1 M $AlCl_3$ aqueous electrolyte.

Figure 3.7a shows the CV profiles of PANI in 1 M $AlCl_3$ aqueous electrolyte in the potential window of 0 V to 0.9 V at a scan rate of 2 mVs^{-1}. In this case also, a pair of very broad cathodic and anodic peaks could be noticed. The cathodic and anodic peaks are centered around 0.35 V (peak E) and 0.4 V (peak F). Figure 3.7b shows the charge-discharge profiles of PANI in 1 M $AlCl_3$ aqueous electrolyte at a current density of 1 Ag^{-1}. Similar to the CV profiles, there are no distinct discharge or charge potential plateaus. The first specific discharge capacitance is 344 Fg^{-1} and this value is 282 Fg^{-1} at the 100th cycle (Figure 3.7c).

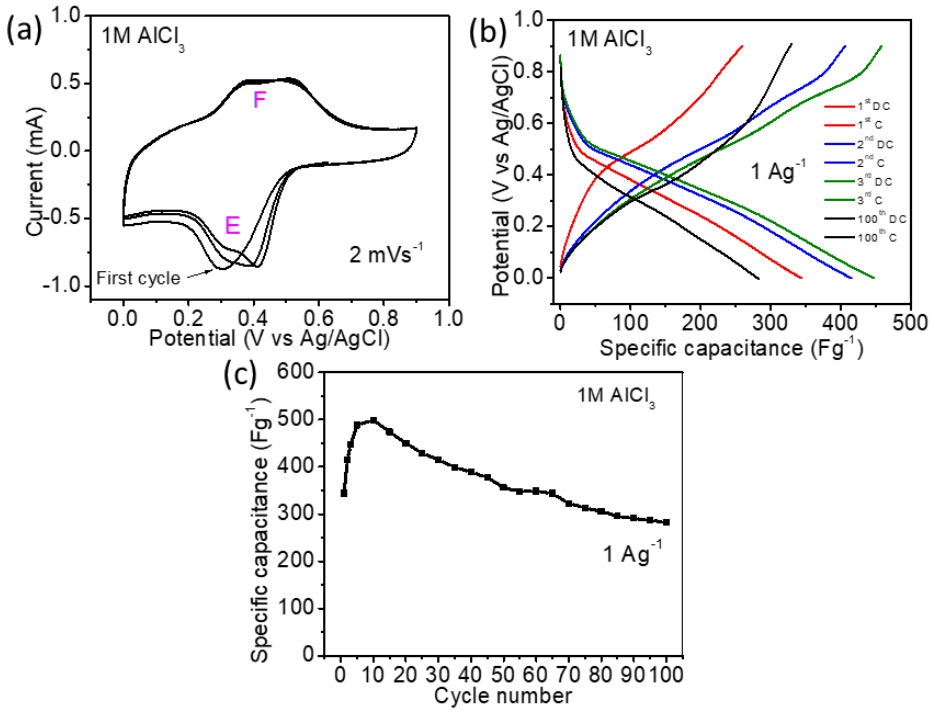

Figure 3.7: (a) CV profiles (b) Discharge-charge profile and (a) Capacity versus cycle number of PANI in 1 M $AlCl_3$ aqueous electrolyte.

The CV and charge-discharge profiles of PANI in the 0.5 M $Al_2(SO_4)_3$ and 1 M $Al(NO_3)_3$ aqueous electrolytes, as shown in (Figure 3.8(a-d)), are almost similar to 1 M $AlCl_3$ aqueous electrolyte. However, as could be seen from (Figure 3.8e), the specific capacitance is higher in case of 1 M $AlCl_3$ aqueous electrolyte than $Al_2(SO_4)_3$ and $Al(NO_3)_3$ aqueous electrolytes . There is an initial hike in the capacitance which may be attributed to the facile accessibility of the electrolyte in the porous structure of the electrodes during initial cycling.

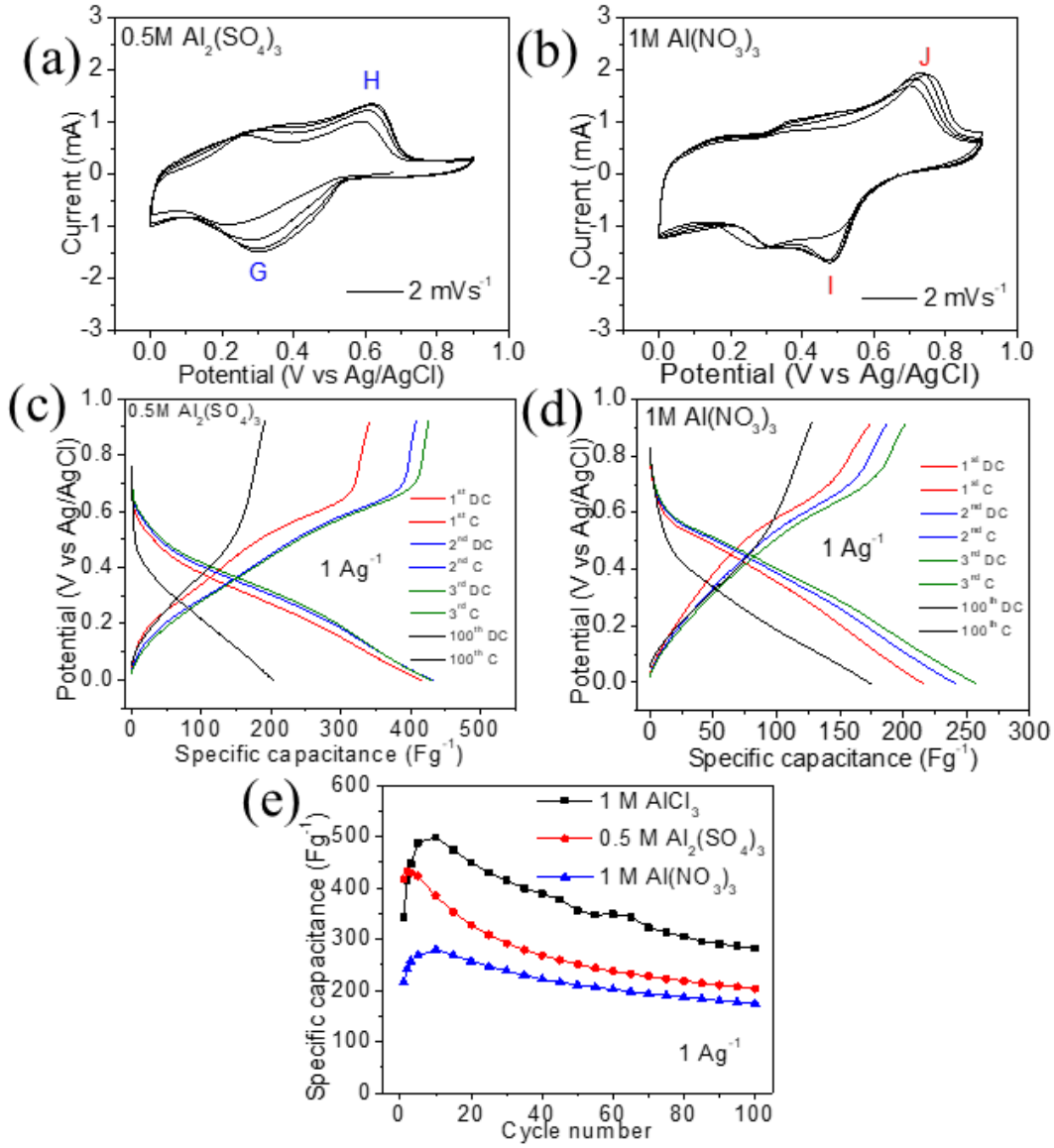

Figure 3.8: CV profiles of PANI for the aqueous electrolytes (a) 0.5 M $Al_2(SO_4)_3$ and (b) 1 M $Al(NO_3)_3$, Charge-discharge profiles of PANI for the aqueous electrolytes (c) 0.5 M $Al_2(SO_4)_3$ and (d) 1 M $Al(NO_3)_3$ and (e) Comparison of long cycling stability of PANI for all the aqueous electrolytes.

The CV data were analyzed using the Randles-Sevcik relationship and the estimated b values for VOA and PANI are close to 0.5 and 1 respectively indicating diffusion and surface mediated charge storage processes (Figure 3.9) [9, 10]. Due to lack of clarity in the cathodic peak of VOA at higher scan rates (Figure 3.10), the anodic peak (C) was considered. However, both the cathodic and anodic peaks were observed even at higher scan rate for the case of PANI (Figure 3.11). Besides, it is clearly evident that the charge-discharge profiles are almost linear, which is apparently a typical characteristic of a capacitor. Since the b value suggests a diffusion process in case of VOA and the charge-discharge profiles are almost linear, VOA could be classified a pseudocapacitive material [11].

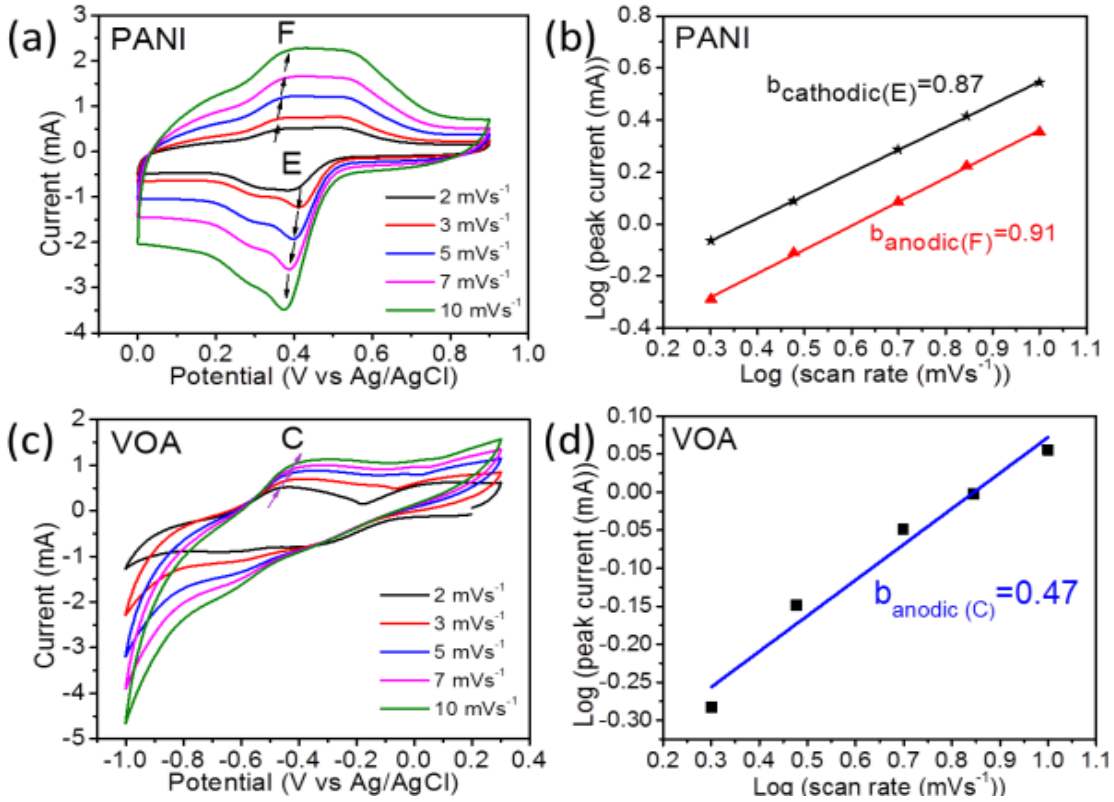

Figure 3.9: CV profiles of (a) PANI and (c) VOA at different scan rates. Plot of log (peak current) vs log (scan rate) for (b) PANI and (d) VOA.

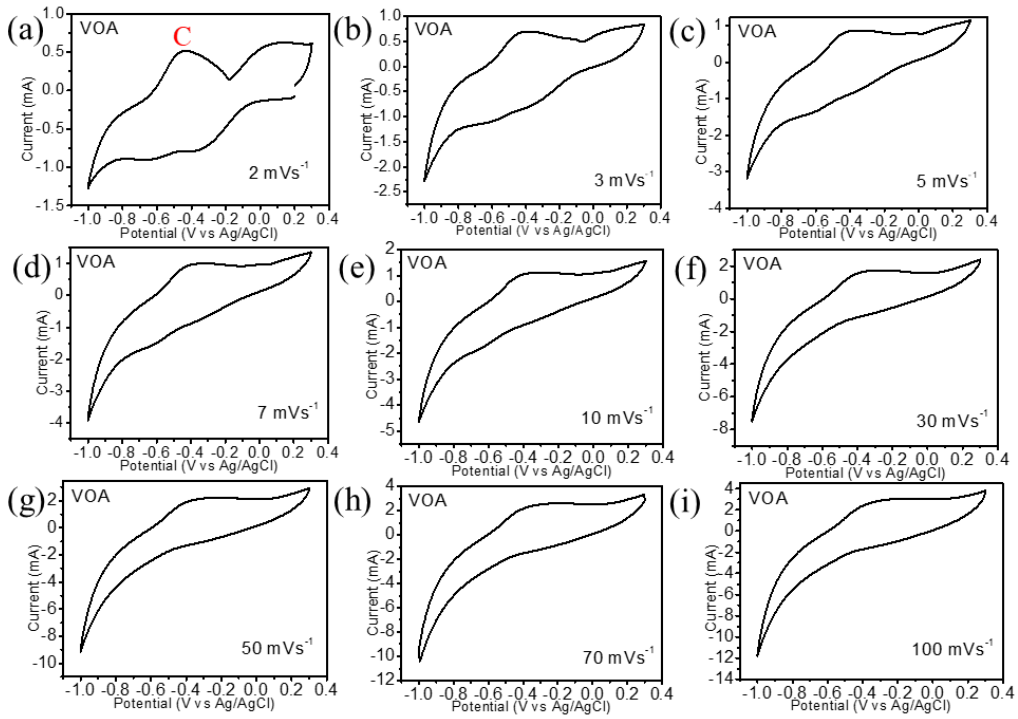

Figure 3.10: CV profiles of VOA in 1 M AlCl3 aqueous electrolyte at different scan rates. [NOTE: it was difficult to identify the cathodic peak in the case of VOA at higher scan rates. Therefore, to calculate the b value, the most distinct anodic peak (labeled as peak C) is considered.]

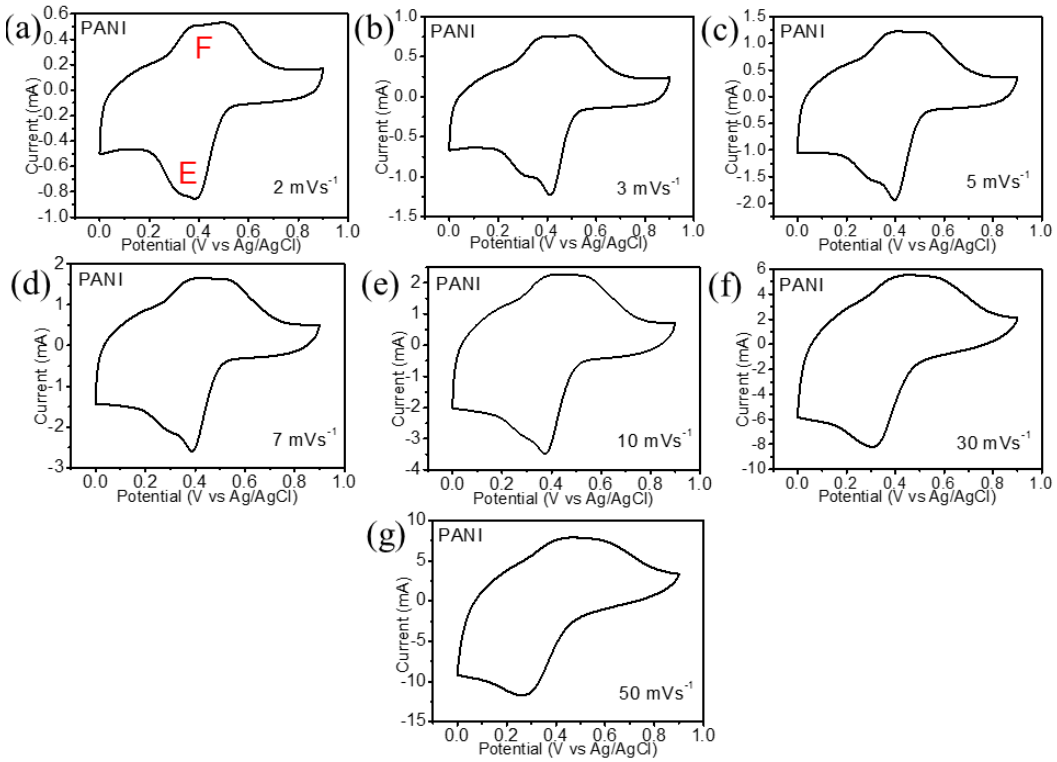

Figure 3.11: CV profiles of PANI in 1 M $AlCl_3$ aqueous electrolyte at different scan rates.

It is to be noted that CV experiments conducted in 1 M HCl and 0.5 M H_2SO_4 solutions indicate electrochemical proton activity of VOA and PANI (Figure 3.12). Therefore, there is possibility of co-insertion of proton together with Al^{3+} ion in VOA and PANI. However, due to very low proton concentration (~ 1 mM) in 1 M $AlCl_3$ aqueous electrolyte, there may be negligible proton insertion/adsorption as compared to Al^{3+} ion.

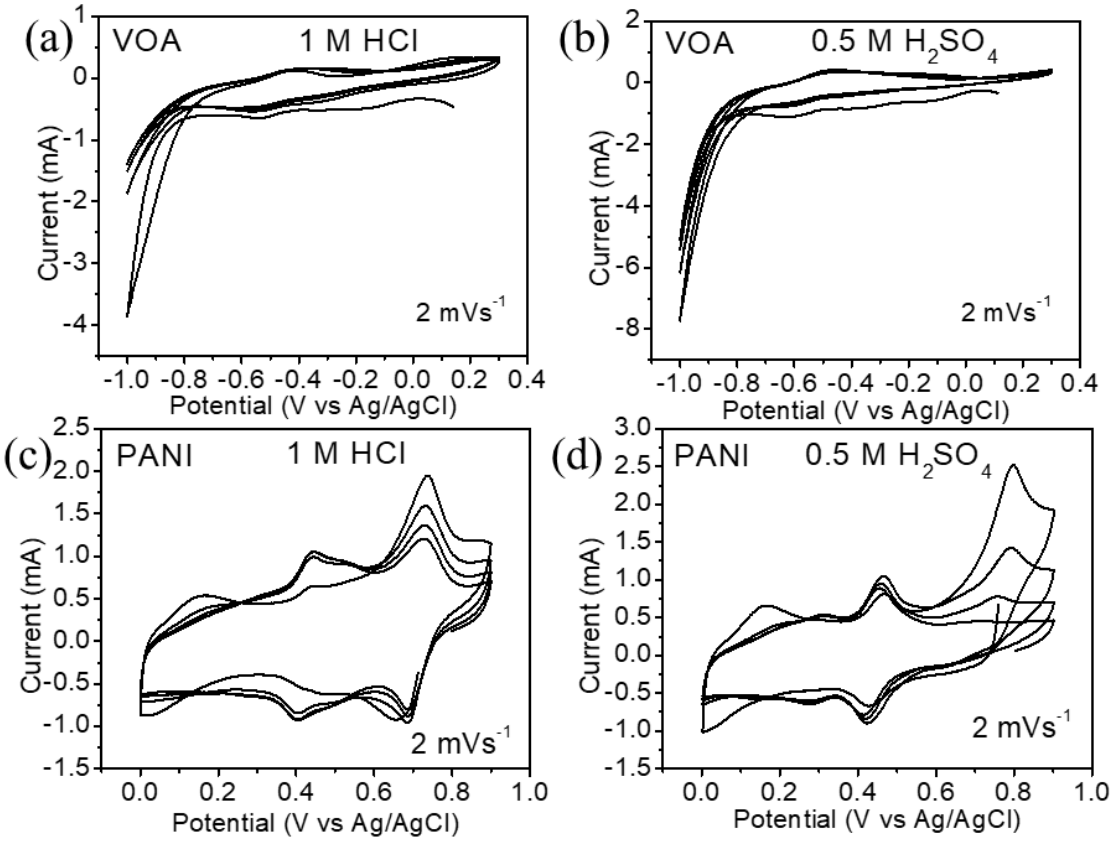

Figure 3.12: CV profiles of VOA in (a) 1 M HCl and (b) 0.5 M H_2SO_4, CV profiles of PANI in (c) 1 M HCl and (d) 0.5 M H_2SO_4.

Finally, electrochemical evaluation on an asymmetric supercapacitor with VOA and PANI as electrodes was performed (Figure 3.13). The electrolyte is 1 M $AlCl_3$ aqueous electrolyte. Initially, a series of CV experiments (scan rate = 2 mVs^{-1}) were conducted to determine a suitable potential window. The experiments were performed in the following potential ranges: (0-1.3) V, (0-1.4) V, (0-1.5) V, (0-1.6) V, (0-1.7) V and (0-2) V (Figure 3.14). It could be noticed that, in the case of (0-1.3) V, there is only one very minor cathodic peak at 0.3 V, whereas the anodic peak is not properly traceable (Figure 3.14a). Contrarily, when the potential window was raised to 1.4 V (Figure 3.14b), there were two very broad cathodic peaks around 0.78 V and

0.38 V. The anodic peak was observed around 0.90 V. On the other hand, the features of CV profiles obtained in the potential windows of (0-1.5) V, (0-1.6) V, (0-1.7) V and (0-2) V are almost similar except slight changes in the peak positions (Figure 3.14 (c-f)).

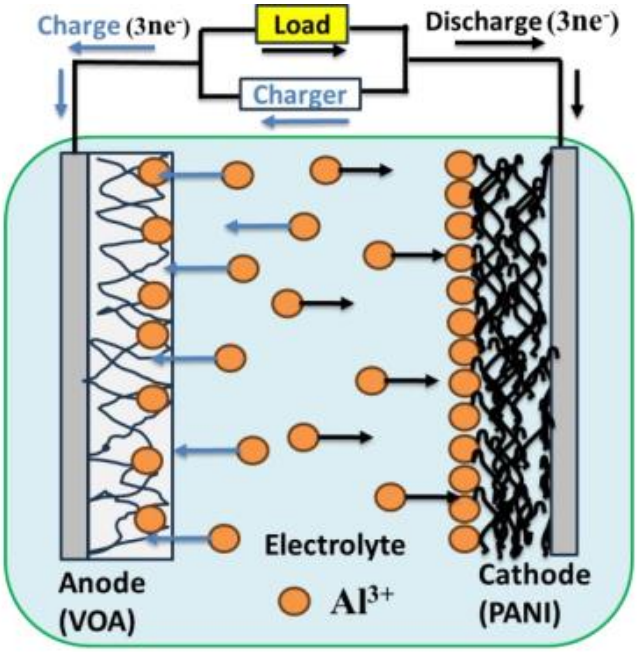

Figure 3.13: Schematic diagram of VOA/PANI cell

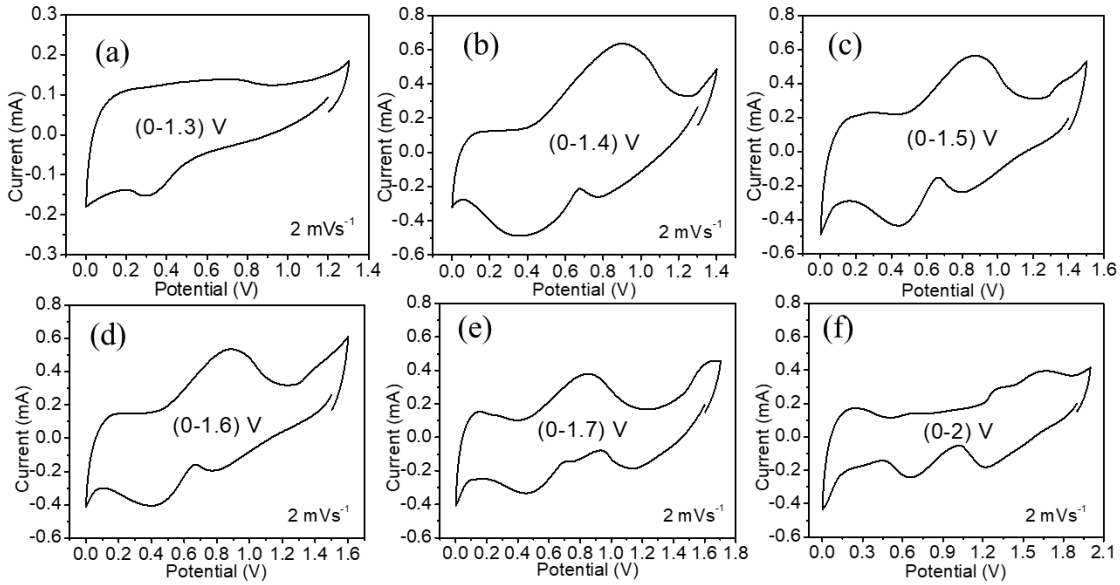

Figure 3.14: CV profiles of VOA/PANI asymmetric supercapacitor in different potential windows.

Figure 3.15 (a-c) represents the charge-discharge profiles of VOA/PANI asymmetric supercapacitor in the potential windows of (0-1.5) V, (0-1.7) V and (0-2) V in 1 M $AlCl_3$ aqueous electrolyte at a current rate of 0.5 Ag^{-1}. Corroborating the

respective CV profiles, the charge-discharge profiles also did not show prominent discharge or charge potential plateaus. Only a kink around 0.5 V and 1 V could be noticed for the discharge and charge profiles respectively. The charge-discharge profiles bear similarity to the potential profiles typically obtained for pseudocapacitive electrodes [14]. The specific discharge/charge capacitance values at the 5th cycle are estimated to be 109 Fg^{-1}/106 Fg^{-1}, 114 Fg^{-1}/114 Fg^{-1} and 132 Fg^{-1}/148 Fg^{-1} for the potential window of (0-1.5) V, (0-1.7) V and (0-2) V respectively.

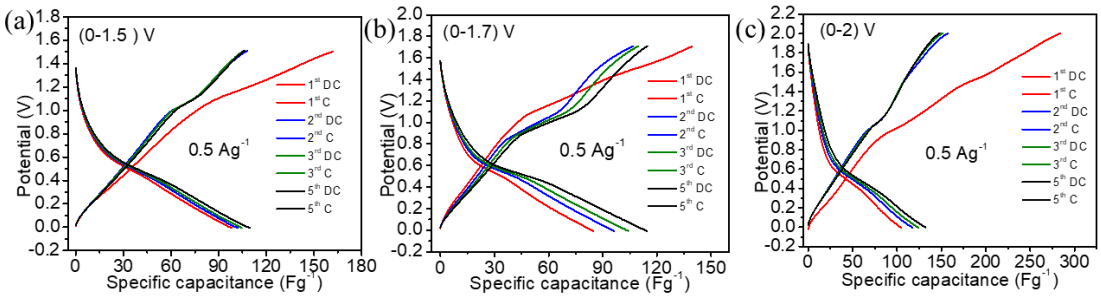

Figure 3.15: Charge-discharge profiles of VOA/PANI in the potential windows of (a) (0-1.5) V, (b) (0-1.7) V, (c) (0-2) V at current density of 0.5 Ag^{-1}.

Overall, as shown in (Figure 3.16 (a-c), and Table 3.1), it is observed that the rate capability of the asymmetric supercapacitor is better for the potential window of (0-2) V. For example, the discharge specific capacitances at current rate of 1.5 Ag^{-1} are 88 Fg^{-1}, 97 Fg^{-1} and 113 Fg^{-1} respectively for (0-1.5) V, (0-1.7) V and (0-2) V. The energy versus power density plot is shown in (Figure 3.17a). For each current density, the values of energy and power density were determined for the 5th cycle. The energy/power density was estimated to be 15 Wh kg^{-1}/750 W kg^{-1} at current density 1.5 Ag^{-1} for the potential window of (0-2) V, whereas these values are 9 Wh kg^{-1}/637 W kg^{-1} and 6 Wh kg^{-1}/562 W kg^{-1} for (0-1.7) V and (0-1.5) V. The asymmetric cell (measured over (0-2) V) also shows good cycling stability over 1000 cycles with specific discharge capacitance of 52 Fg^{-1} at current density of 1 Ag^{-1} (Figure 3.17b)

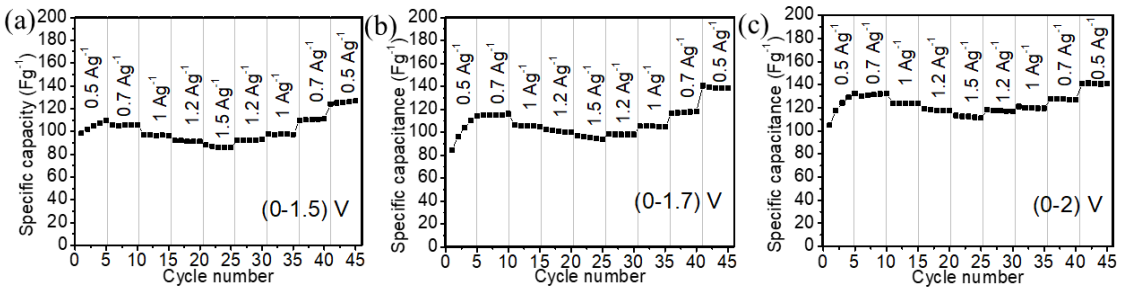

Figure 3.16: Rate capability of VOA/PANI in the potential windows of (a) (0-1.5) V, (b) (0-1.7) V, and (c) (0-2) V.

Table 3.1: Comparison of the difference of specific capacitance between 5th and 45th cycle for the potential windows of (0-1.5) V, (0-1.7) V and (0-2) V at current density of 0.5 Ag^{-1}.

Potential window (V)	5th discharge specific capacitance (Fg^{-1})	45th discharge specific capacitance (Fg^{-1})	Difference (Fg^{-1})
(0-1.5)	109	126	17
(0-1.7)	114	138	24
(0-2)	132	140	8

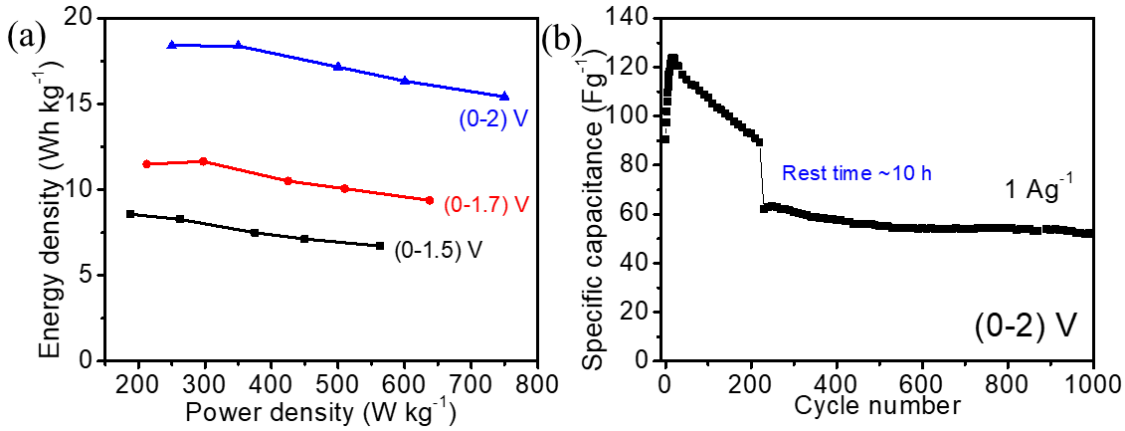

Figure 3.17: (a) Energy density vs power density plot and (b) Long term stability curve in the potential window (0-2) V.

Finally, a physical application was demonstrated in (Figure 3.18), where we could light up a LED for 5 minutes using VOA as anode and PANI as cathode in 1 M $AlCl_3$ aqueous electrolyte.

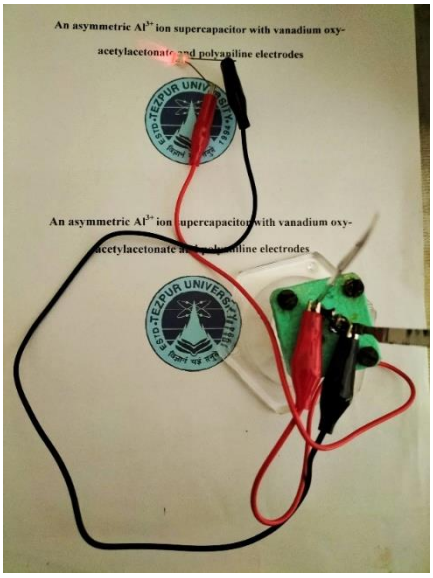

Figure 3.18: Snapshot of the demonstration of the VOA/PANI cell to light up a LED light

3.4 Conclusion

In summary, it was shown that VOA and PANI can store Al^{3+} ion in aqueous electrolyte. The specific capacitance values for VOA and PANI are 182 Fg^{-1} and 282 Fg^{-1} respectively at current density of 1 Ag^{-1}. The asymmetric cell based on the VOA and PANI electrode shows good electrochemical stability and it shows better performance in the potential range of (0-2) V. The cell delivers an energy and power density of 15 Wh kg^{-1} and 750 W kg^{-1}. This study is a unique example of Al^{3+} ion based organic supercapacitor.

3.5 References

[1] Romero, P. G., Chojak, M., Gallegos, K. C., Asensio, J. A., Kulesza, P. J., Pastor, N. C., and Chantu, M. L. Hybrid organic-inorganic nanocomposite materials for application in solid state electrochemical supercapacitors. *Electrochemistry Communication*, 5: 149-153, 2003.

[2] Nandi, S., Yan, Y., Yuan, X., Wang, C., He, X., Li, Y., and Das, S. K. Vanadyl ethylene glycolate: A novel organic-inorganic electrode material for rechargeable aqueous aluminum-ion battery. *Solid State Ionics*, 389: 116085, 2023.

[3] Vujkovic, M. J., Etinski, M., Vasic, B., Kuzmanovic, B., Bogdanovic, D. B., Dominko, R., and Mentus, S. Polyaniline as a charge storage material in an

aqueous aluminum-based electrolyte: Can aluminum ions play the role of protons? *J. Power Sources*, 482: 228937, 2021.

[4] Nagaraj, R., Pakhira, S., Aruchamy, K., Yadav, P., Mondal, D., Dharmalingm, K., Kotrappanavar, N. S., and Ghosh, D. Catalyzing the intercalation storage capacity of aqueous zinc-ion battery constructed with Zn (II) preinserted organo-vanadyl hybrid cathode. *ACS Appl. Energy Mater.*, 3: 3425, 2020.

[5] X. Wang, X. Bi, S. Zheng, S. Wang, Y. Zhang, H. Du, J. Lu, High rate performance and ultralong cycle life enabled by hybrid organic inorganic vanadyl ethylene glycolate for lithium-ion batteries. *Adv. Energy Mater*. 8: 1801978, 2018.

[6] Wang, X., Wang, S., Zhang, Y., and Du, H. Organic vanadium oxy-acetylacetonate as electro-active anode material with high capacity and rate performance for lithium-ion batteries. *J. Mater. Sci*. 53: 9701-9709, 2018.

[7] Qiao, J., Tao, F., Wei, Q., Zhang, X., Xie, W., Li, X., and Yang, J. Electrochemical properties of aluminum ion batteries with emeraldine base polyaniline as cathode material. *J. Electroanal. Chem*. 929: 117102, 2023.

[8] Palsaniya, S., Nemade, H. B., and Dasmahapatra, A. K. Mixed surfactant-mediated synthesis of hierarchical PANI nanorods for an enzymatic glucose biosensor. *ACS Appl. Polym. Mater*. 1: 647-656, 2019.

[9] Li, A., Wei, Z., Wang, Y., Zhang, Y., Wang, M., Zhang, H., Ma, Y., Liu, C., Zou, J., Ge, B., Cheng, F., and Yue, Y. Flexible quasi-3D zinc ion microcapacitor based on V_2O_5-PANI cathod and MXene anode. *Chem. Eng. J*. 457: 141339, 2023.

[10] Wei, Z., Zhang, H., Li, A., Cheng, F., Wang, Y., Zhang, Y., Wang, M., Gao, B., Cheng, Y., Liu, C., Liu, N., Ma, Y., Ge, B., Gao, Y., and Yue, Y. Construction of in-plane 3D network electrode strategy for promising zinc ion storage capacity. *Energy Storage Mater*. 55: 754-762, 2023.

[11] Gogotsi, Y., and Penner, R. M. Energy storage in nanomaterials-capacitive, pseudocapacitive, or battery-like? *ACS Nano,* 12: 2081-2083, 2018.